CHALMERS

Light Assisted CO_2 Conversion Using Nanostructured Model Catalysts

Master of Science Thesis in Applied Physics

ANDREAS ERIKSSON

Department of Applied Physics
Division of Chemical Physics
CHALMERS UNIVERSITY OF TECHNOLOGY
Gothenburg, Sweden, 2011
Master Thesis 2011:11

Abstract

Modern society is built on energy, figuratively speaking. Given the consequences of increased CO_2-emissions, due to combustion of fossil fuels and accidents in for example nuclear power, it is clear that new ways of producing this energy is needed to satisfy our future energy needs. One possible energy source is the storing of solar energy in the form of chemical fuels, to overcome its otherwise intermittent nature. The light assisted conversion of CO_2 and water into short hydrocarbons has been proposed as a viable candidate.

In this project we investigate whether a more well defined sample structure can be utilized to scrutinize the specifics of light assisted CO_2-conversion. Two type types of sample structured were fabricated utilizing nanofabrication techniques. Both consisted of a flat TiO_2 surface, in anatase configuration, with catalyst metal particles deposited on it. The first utilized cluster formation and material growth properties when depositing film with thickness of $\sim$1nm. The second type was fabricated using Hole mask colloidal mithography and shadow evaporation techniques to define dual metal catalyst particles on the TiO_2 surface. While the first type of samples showed no visible sign toward hydrocarbon production, the second type showed tendencies towards methane production albeit with levels too small to be considered conclusive evidence.

Keywords: Photocatalysis, Photochemistry, Carbondioxide, CO2-conversion, Titaniumdioxide,

Acknowledgements

I like to thank my fiancee Satoe Yoshinari for all her support and for being her wonderful self during this project. I would like to extend my gratitude to my supervisor Björn Wickman for his great support and guidance during this project. I would also like to thank my examiner as well as co-supervisor Michael Zäch for all his help and support as well as his great patience with me during the time it took for me to finish this report. I would also like to thank Dinko Chakarov, Raja Sellappan and Rafael Martins for letting me utilize their equipment for my experiments as well as their teaching and assistance in operating it. Last but not least I am grateful to my cat Tittu for her excessive judgemental staring that has guilted me into working harder.

Contents

Chapter 1

Introduction

1.1 The growing pains of society, our increasing demands in energy

The continued growth of humanity brings with it its own set of problems. One of these problems is based on that our society is built on energy, figuratively speaking, and as society continues to grow it will require more and more energy to sustain itself. As an illustrative example; in the year 1973 the world's total energy consumption was 4,674 Mtoe (toe: Tonne of Oil Equivalent). By year 2009 this figure had increased to 8.353 Mtoe [1]. Approximately 75 % of the world's energy supply is produced through the use of fossil fuels, such as oil, coal and natural gas. Nuclear power accounts to 5.8 % and the rest is divided amongst hydropower and bio-fuels. [1] During combustion of fossil fuels CO_2 is released. So it may not come as a surprise that the emissions of CO_2 from fossil fuel combustion increased accordingly from 15 643 Mt to 29 381 Mt over the same time period [1]. CO_2 is a greenhouse gas and is thought to be a major reason behind the green house effect.

The vast emissions of CO_2 into the atmosphere due to the use of fossil fuels and the impact of nuclear disasters such as Chernobyl and, more recently, the Fukushima incident, remind us that new ways of producing energy are required to fulfill our future needs. This will become more and more crucial as society continues to grow. Or as the adage goes "A picture is worth a thousand words, now see figure 1.1" . It serves as a good illustration of the energy consumption in the world today.

The properties we would want from the world's future energy source include: abundant primary energy source (fuel), low impact on the environment or preferably none at all, scalable process, safe and economically plausible.

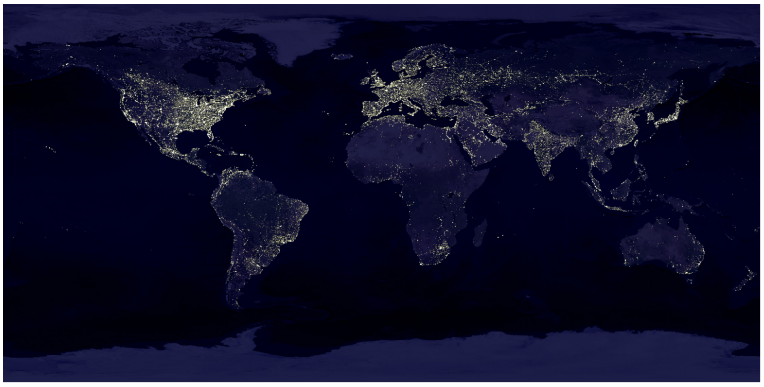

Figure 1.1: Earth as seen from space during night. It serves as an illustrative image of the state of the world today when it comes to energy consumption

1.2 Solar energy - The holy grail of energy production

In the previous section, some desired properties for the world's future energy source were listed. One possible candidate for such an energy source would be solar energy. Approximately 3,850,000 EJ of solar energy reaches our earth's surface every year [2]. An astonishingly large amount of energy which amounts to approximately 10,000 times the world's total energy consumption. Today, there are already commercial solar energy producing systems available, e.g. solar collectors and solar photo-voltaic cells for heat and electricity production. However, an obvious problem with direct solar energy conversion is the fact that it only works when the sun is shining. We want to be able to store solar energy for a rainy day, so to speak.

1.3 CO_2 as a possible fuel source

A possible way of storing solar energy is to use it to form chemical compounds. In this situation, the energy is stored in chemical bonds. Recent interest in the field of photocatalysis, has shown a promising candidate in the light assisted conversion of CO_2 and water into short hydrocarbons, for example methane and methanol. The reactants would be CO_2 and water, both of which are abundant in nature. Upon combustion of the produced hydrocarbons, the stored energy would be released together with CO_2 and water, making it a completely renewable energy source, provided that CO_2 can be captured.

1.4 Project purpose and aims

Earlier publications in this area [3][4] show that the light assisted conversion of CO_2 and water into short hydrocarbons is indeed a feasible approach. However, the process suffers from low quantum yield and the mechanisms involved are currently not fully understood. Understanding of the physical mechanisms is crucial if efficiency of the process is to be increased. This project seeks to

investigate whether a more well-defined sample structure can be used to scrutinize the specifics of photocatalyzed conversion of CO_2 and water into short hydrocarbons.

Chapter 2

Background

2.1 Redox-reactions and Catalysed reactions

2.1.1 Introduction to chemical reactions

A redox-reaction (reduction-oxidation-reaction) refers to the type of chemical reaction where the reactants change their oxidation state. As a simplified description of the concept, reduction and oxidation can be seen as reactions involving gain and loss of electrons. Reduction refers to a reaction where the reactant receives electrons and oxidation to a reaction when they lose electrons. Note however that a reaction does not need to involve charge transfer of one whole elemental charge for it to be called a redox-reaction. Reactions where the relative charge concentration is changed are also considered redox-reactions as in the case of the forming of covalent bonds. For example the oxidation of CO into CO_2.

What decides whether a reaction is thermodynamically favorable is the difference between the Gibbs free energy, ΔG, between the reactants and the products. A negative ΔG means that there is a driving force to form the products, i.e. the reaction is thermodynamically favorable. Most reactions consist of multiple steps and involve transition states. These transition processes may not be energetically favorable even if the overall reaction is. Or in other words, even if the overall reaction has a negative difference in free energy does not mean that each sub process will have a negative difference in free energy. Most chemical reactions have a so called activation barrier or activation energy. This is the energy that needs to be provided to the reactants for them to perform a given chemical reaction. An illustration of a reaction with activation barrier (E_A) and overall change in energy (ΔE) can be seen in figure 2.1. The activation energy is why, for example gasoline does not spontaneously combust even though the reaction is obviously energetically favorable. To overcome the activation barrier, energy must be supplied to the system.

As an illustrative example the reactants A and B are made to react with each other. The difference in energy between the initial state (1), before any reaction has occurred, and the product (3) is the overall change in energy of the reaction. The difference in energy between the initial state (1) and the step with

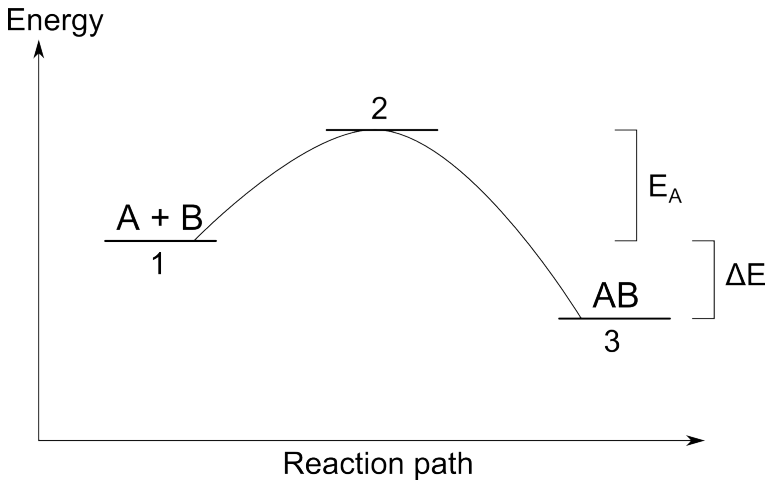

Figure 2.1: Energy diagram of a general chemical reaction with a transition state. E_A: Activation energy, ΔE: Overall change in energy

the highest relative energy (2) is called the activation energy of the reaction. Energy larger than the activation energy must be supplied to the system for the reaction $A + B \longrightarrow AB$ to take place.

2.1.2 Heterogeneous Catalysis

The concepts of catalysis has been known since the beginning of the 19:th century. Applications based on heterogenous catalysts have existed since the beginning of the 19:th century with the invention of the platinum based Dobereiner lamp. The lamp was actually a lighter that produced a flame through platinum catalyzed oxidation of H_2[5]. Being formally defined by Berzelius in the 1830's, catalysis has been a well researched area and conceptually the mechanisms are well understood [6].

A catalyst is defined as a substance or material that increases the reaction rate for a given chemical reaction without being consumed in the process. There are basically two forms of catalysis, homogeneous catalysis where the catalyst and reactants are in the same phase, and heterogeneous catalysis where the catalyst and reactants are in different phases. This work is limited to the latter.

A heterogenous catalyst is basically a substance where the chemical reaction takes place on an active site on the catalysts surface. In general, when people think about catalysts they tend to think about a heterogeneous catalyst. Probably because of the car part aptly named "the catalyst". The catalyst of a vehicle, amongst other reactions, catalyze the chemical conversion of carbonmonoxide into carbondioxide, which would be the proverbial lesser of two evils.

2.1.3 Mechanisms of catalysts

The general definition of a catalyst is fairly easy to understand but to give a more indepth explanation to how a catalyst works is not a trivial task. The specific working mechanisms of different catalysts and different reactions are in general not the same. For example, different chemical reactions may happen at different sites on the catalyst and the transition steps will not be the same. However from a general point of view, most heterogeneous catalysts follow the same principle.

Imagine the simple situation, discussed in section 2.1.1 where we have a first order reaction where reactants A and B form the product AB. In the uncatalyzed reaction there will be an activation barrier to overcome due to the energy related to transition. What a catalyst do in general is binding one or both of the reactants to its surface (see figure 2.2. This opens up a new set of transition steps (states 2C and 3C) that leads to the same end product but with lower energy related to them; effectively reducing the activation barrier for the reaction. In general, a catalyst can increase the reaction rates but the reaction mechanism can become more complex.

The overall change in free energy between reactants and products are not

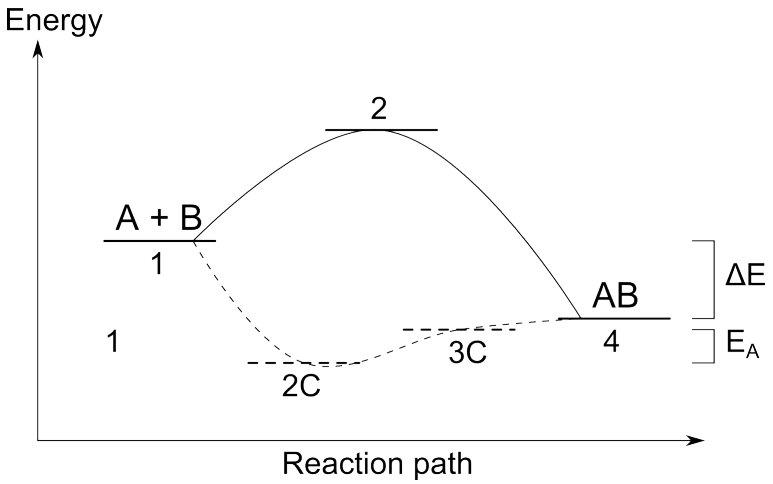

Figure 2.2: Free energy diagram of a general reaction compared to the same but catalyzed reaction (dashed line)

changed however. I.e. a catalyst cannot change if a reaction is thermodynamically favorable or not. It can only change the reaction rate [7].

2.2 Catalysts for CO_2 conversion

During the combustion of chemical fuels, energy is released in the reaction making ΔE (difference in energy between product state and reactant state) negative. In most cases there is also an activation barrier that needs to be overcome for the reaction to take place. All chemical reactions are in theory reversible i.e. it

is possible to go from product back to reactant given that sufficient energy is provided so the system can go up to the higher state. There are different ways of providing this energy. In "normal" reactions the energy is in the form of heat, in electrochemistry the electrons receive energy through an applied electric field and in photochemistry energetic electrons are created through photoexcitations. Just as in the downhill reaction there is an activation barrier that needs to be overcome or lowered using various catalysts. In this section, two catalysts for hydrocarbon production through CO_2 conversion will be discussed.

2.2.1 Use of copper in CO_2 reduction reaction and platinum for water oxidation

When dealing with complicated reaction systems, for example TiO_2 based photocatalysts, it is very likely that the reaction will not be as simple as described as in figure 2.2. Not only will the single reaction paths be more complicated but there will be more than one possible such path and therefore more than one possible product. For a given system, the reaction that is most likely to happen will give rise to the majority product of the system. However small formations of other products may still be present. For example, photoinduced CO_2-conversion taking place on a pure TiO_2 is reported to give rise to mostly methane, hydrogen and CO [3]. Introducing catalyst materials such as Cu and Pt into the system may not only improve turnover rates but may also alter the selectivity of the photocatalyst. For example, it has been reported that when adding Pt onto TiO_2 the photocatalyst produce alot of hydrogen, some methane, some traces of CO and some formation of alkanes and olifins [3]. With the same type of TiO_2-based photocatalyst but with Cu, the production of hydrogen, alkanes and olifins is decreased while the production of CO and methane is increased.

Platinum is a well known catalyst in both electrochemistry as well photochemistry and has been used extensively in research in the field of hydrogen production/water splitting. Copper has been shown to catalyze the reduction of CO_2 into short hydrocarbons. In fact only copper and its alloys are known to be able to catalyze the electroreduction of CO_2 into hydrocarbons with high efficiency and selectivity [8].

2.3 Semiconductors

2.3.1 Introduction to semiconductors

There are essentially two useful ways of defining what a semiconductor is. In solid state physics a semiconductor is often defined as a material with resistivity between 10^{-2} and 10^{9} Ωcm [9]. The other way of defining a semiconductor is by defining it as a material with a band gap between its valence band and conduction band in the range of zero to about 4 eV [10]. The band gap is defined as the difference in energies between the conduction and valence band edges i.e. the minimum amount of energy required to excite an electron from the valence band to the conduction band. A schematic of the band levels for a semiconductor can be seen in figure 2.3. Neither of the two aforementioned definitions are very rigorous since for example the resistivity of a semiconductor is strongly

temperature dependent.

As far as general descriptions go, the image of the semiconductor having a

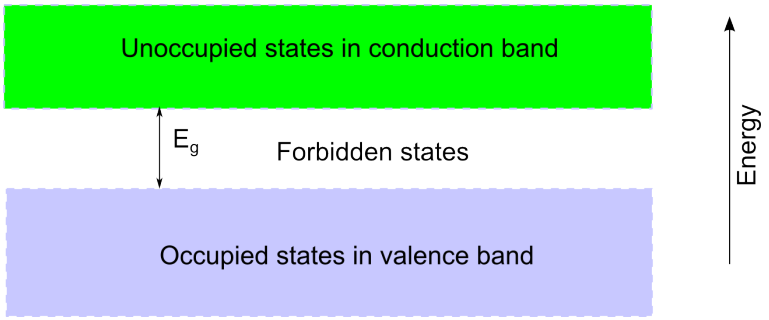

Figure 2.3: Schematic of the band levels of a semiconductor. E_g denotes the band gap energy i.e. the minimum energy required to excite an electron from the valence band to the conduction band

band gap in the eV range is important to understand what happens when light is absorbed by the material. When light with energy higher than the bandgap energy hits a semiconductor, an electron from the valence band has the possibility to be excited to the conduction band. The interaction between light and the crystal lattice of a semiconductor will be discussed further in 2.4.1.

It is also important to note that the electronic properties of a material are partly based on which elements are included in the crystal lattice but also on the crystal structure of the material. Different structures can lead to vastly different properties of that material. A well known example is the different crystal structures of carbon. For a semiconductor, changes in crystal structure can lead to different bandgap energies, band structure and chemical properties amongst other things. The consequences for this project will be discussed further below.

2.3.2 Titanum dioxide

Titanium dioxide (Titania or TiO_2) is a popular semiconductor in the field of surface physics. Especially in the field of photocatalysis, which we will discuss further in 2.4, has TiO_2 been of special interest. The work by Fujushima and Honda [11], where they showed that TiO_2 can be used for hydrogen production through photoinduced water splitting, is mentioned as the starting point for the interest in TiO_2-based photocatalysis.

There are three stable polymorphs of TiO_2; Rutile, anatase and brookite. Amongst the three configurations, rutile has the lowest energy in bulk [12] and it is the stable high temperature configuration of bulk TiO_2. A stick and ball schematic of the crystal structure can be seen in figure 2.4.

Anatase has the lowest energy in nanoparticles smaller than approximately 14 nm [12]. The anatase phase is of special interest since it shows higher photocatalytic activity than the two either polymorphs in many cases [14]. A schematic

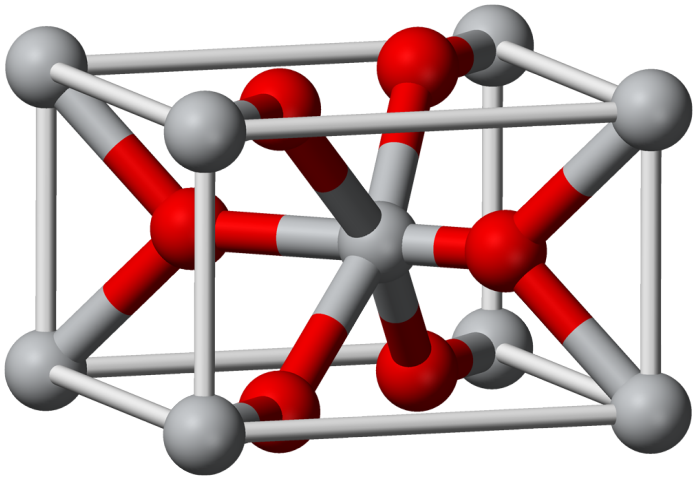

Figure 2.4: Stick and ball schematic of the rutile unit cell [13]. Bright balls represent Ti-atoms and dark balls represent O-atoms.

stick and ball model of the anatase unit cell can be seen in figure 2.5.

The obvious conclusion we can draw from figures 2.4 and 2.5 is that they

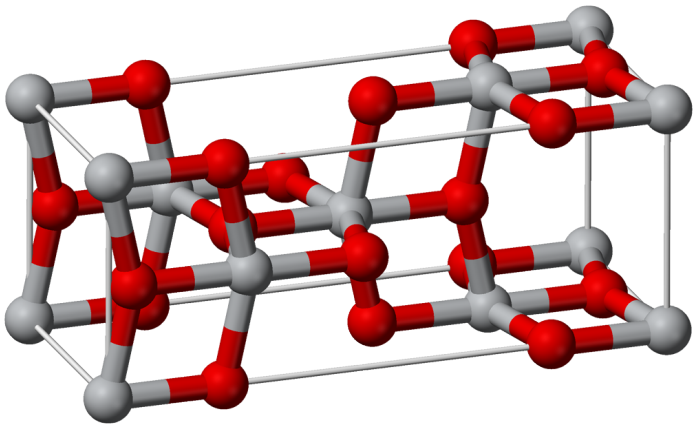

Figure 2.5: Schematic stick and ball model of the anatase unit cell. The brighter balls represent Ti-atoms and the darker represent O-atoms [15].

are different. This difference in crystallographic configuration leads to different energetics as well as different band structure of the TiO_2. The band gap energy is 3.0 eV and 3.2 eV for rutile and anatase resp. The relative band structure of the two polymorphs can be seen in figure 2.6.

What makes this material so interesting is its properties related to photo-

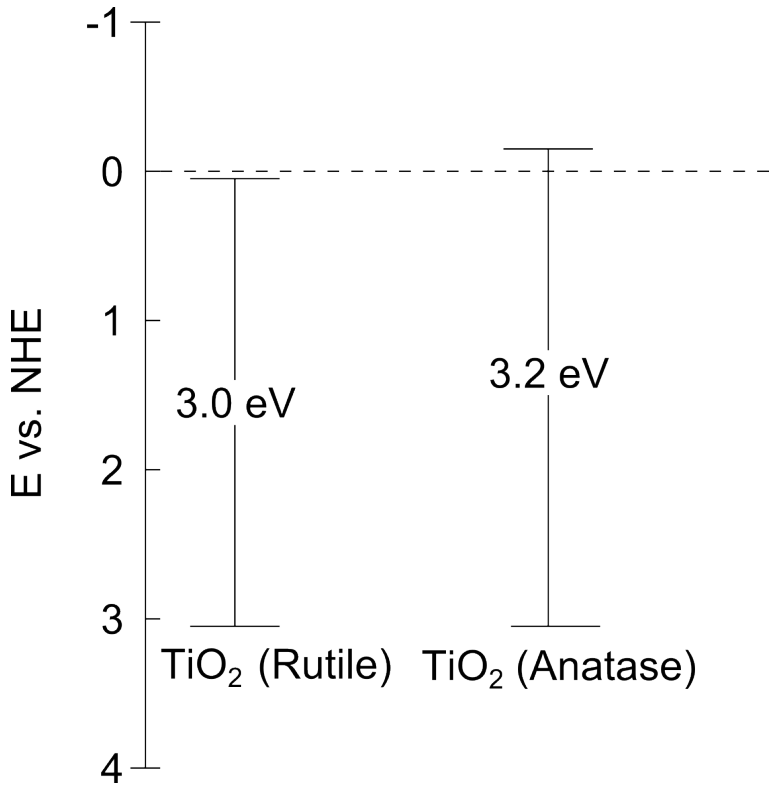

Figure 2.6: Position of band edges of rutile and anatase TiO_2. Values taken from article [16]. NHE stands for "Normal Hydrogen Electrode" . Noticeable is the higher reduction potential for anatase than for rutile TiO_2.

catalytical applications. First of all TiO_2 has a wide band gap making it a stable semiconductor. It is especially an interesting candidate for semiconductor based light induced CO_2-conversion since the band structure allows for both water oxidation as well as CO_2-reduction, at least in theory. How the band structure and band gap energy affects selectivity and possible reaction will be discussed further in 2.4.2.

The brookite structure has been omitted from this discussion on purpose, mainly because it is barely mentioned in the literature in photochemistry contexts. We therefore concentrate on the rutile and anatase structures.

2.4 Photocatalysis

2.4.1 Photo excitation, charge diffusion and recombination

In this section we will discuss further what happens when a semiconductor is irradiated with light. Ideally a semiconductor is transparent to light with energy

less than that of the band gap energy. This is because there are no available states that an electron in the valence band can be excited to.

However, if a photon with energy larger than that of the band gap energy is absorbed by the semiconductor, an electron from the valence band can be excited to the conduction band creating an electron hole pair in the conduction band and valence band. The life time of excitations inside TiO_2 is believed to depend on the structure of the crystal. Measurements has shown that it is of the order of about 10 ns [17] after which the electron hole pair will recombine. The majority of recombination events are thought to be non-radiative in nature, for example, through thermalization, i.e. the energy is dissipated as heat. An illustrative image can be seen in figure 2.7.

During the life time of the electron hole pair the individual charge carriers can be seen as free particles and they are able to diffuse in the semiconductor. If the charge carriers reach the surface they can get trapped in surface states from where they can take part in photochemical reactions with molecules present there. The charge carriers can also become trapped inside the bulk material for example at grain boundaries and in impurity induced states.

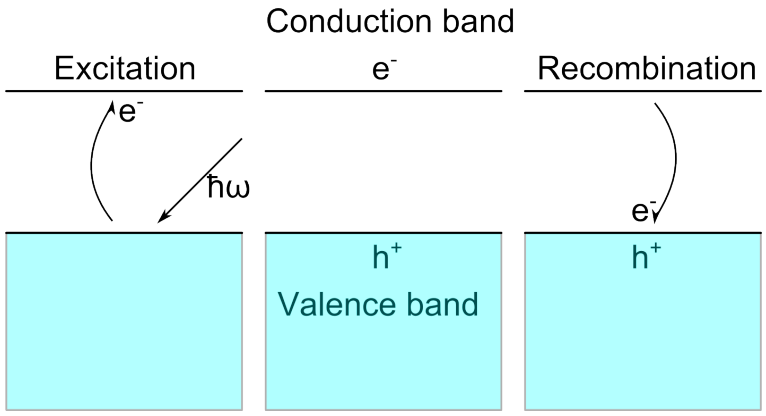

Figure 2.7: Illustration of the excitation, diffusion and recombination events of a semiconductor

2.4.2 Effects of Band structure

In 2.3.2 it was mentioned that a wide band gap is preferential since the band structure affects possible redox-reactions occurring on the surface. This statement is somewhat of an oversimplification so it will require some explanation.

The reactions involved in light induced conversion of CO_2 and H_2O on TiO_2 based photocatalysts all start with charge separation in the semiconductor due to absorption of incoming light. As was discussed earlier the separated electrons and holes will diffuse in the semiconductor until they recombine or reach the

surface of the material. If they reach the surface they can participate in redox-reactions. Obviously, there are no "jack of all trades" amongst semiconductors when it comes to possible reactions that can occur, so the question is what property decides which possible redox-reactions that can occur.

Part of the answer to this question is the band structure of the semiconductor. To illustrate this we look at the case when an electron moves from the donor material (TiO_2) to an acceptor molecule (CO_2) adsorbed on the surface (see figure 2.8).

The valence band edge is the so called "reduction potential" of the semiconductor. Basically, this energy has to be larger than that of the lowest unoccupied molecular orbital (LUMO) of the acceptor molecule for a reduction reaction to take place. A conceptual image could be obtained by treating the situation as a standard standing wave problem and solve the time independent Schrödinger equation for each of the situations with $E_{VB} > V_{LUMO}$ and $E_{VB} < V_{LUMO}$ respectively.

The oxidation reaction can also be seen in the same conceptual way on how the

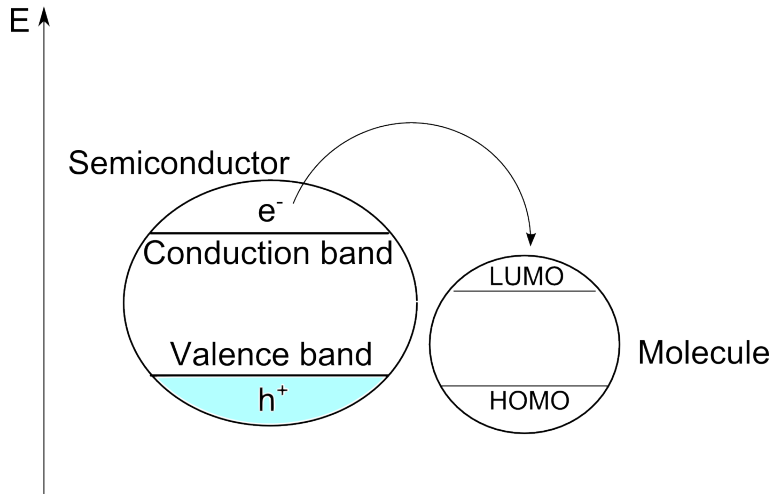

Figure 2.8: Schematic of photo induced reduction of CO_2. An electron has been excited from the valence band into the conduction band. Since the VB is higher than the LUMO of the molecule it is energetically possible for the electron to jump to the LUMO of the molecule thus reducing it, given the right circumstances.

oxidation potential influences possible reactions. One usually mentions it as a hole that moves from the semiconductor to the molecule, but since protons cannot leave the surface one can think about it as an electron leaving the HOMO of the molecule to recombine with the hole in the valence band. In order for such a transfer to take place the HOMO of the molecule must have higher energy than the valence band of the semiconductor. Obviously the aforementioned image is a simplification. In reality, reduction and oxidation may not take place through direct charge transfer. A lot of research in the field today is dedicated

to investigating how oxygen, both dissociated O_2 and oxygen vacancies in the TiO_2 lattice, is involved in the photoreactions [17].

2.4.3 Reaction path of photocatalytic CO_2 conversion into hydrocarbons

Several different reaction paths for the photocatalytic conversion of CO_2 into methane and methanol have been suggested. The general trend in the literature seems to point toward the formation of HCOOH (formic acid) as a pre-step to methane and methanol[3, 4]. A theoretical study of how the electrochemical reduction of CO_2 on copper takes place, suggests that the formation of HCOOH is indeed a part in the reaction path of methane production[8]. Their approach is to look at one elementary step at a time, i.e. the transfer of one proton and one electron a time. They propose the following reaction pathway for methane production, at a potential of -0.74V vs. CHE (Computational hydrogen electrode):

$$CO_2 + H^+ + e^- \longrightarrow COOH \tag{2.1}$$
$$COOH + H^+ + e^- \longrightarrow HCOOH \tag{2.2}$$
$$HCOOH \longrightarrow CO + H_2O \tag{2.3}$$
$$CO + H^+ + e^- \longrightarrow CHO \tag{2.4}$$
$$CHO + H^+ + e^- \longrightarrow CH_2O \tag{2.5}$$
$$CH_2O + H^+ + e^- \longrightarrow CH_3O \tag{2.6}$$
$$CH_3O + H^+ + e^- \longrightarrow CH_4 + H_2O \tag{2.7}$$

However, one must note that the calculations in [8] are done for an electrochemical reaction while our project deals with photochemical reactions in gas phase. Conceptually, photocatalysis and electrochemistry are similar. In photocatalysis the electron get their energy from photon absorption events and in electrochemistry the energy is provided by an external electrical potential. It is also worth noting the fact that a theoretical model does never produce better results than the assumptions it is based on.

2.5 Introduction to nanofabrication

Nanofabrication, as the name implies, refers to the fabrication or manufacturing of something on the nanometer level. The following introduction section is meant to give a short background to the reader of the different fabrication techniques involved in this project. This so that people unfamiliar with the processing techniques utilized can still follow the arguments in later sections. If the reader is familiar with nanofabrication they can skip this introduction.

2.5.1 Lithography

Anyone who has tried threading a string through the head of a needle understands the problem of handling and manipulating small things. Self evidently, this is an even bigger issue on the nanometer scale. Direct manipulation is extremely difficult and if possible it suffers from not being scalable, making it unpractical for mass production.

Lithography in nanofabrication is a collective term for many different techniques used to define structures on the nanometerscale. For example UV-lithography utilizes the creation of a deposition mask by exposing desired areas of the mask to UV-light, as a way of defining patterns. Exposed areas undergo chemical reactions making them easier or more difficult to dissolve when subjected to developer chemicals. The result is a mask that decides which areas can be reached by, for example, material deposition. Another example is electron beam lithography that follows the same principle as UV-lithography but a focused electron beam is used instead of UV-light. The mask material is called a resist.

2.5.2 Resists

Resists are usually polymer substances and can be used as sacrificial layers in some lithography processes. These polymers can be dissolved by external means, for example by exposing them to solvents (sometimes called developers) or through plasma etching. The structure of the polymer can be affected by, for example subjecting it to UV-light, which can cause crosslinking or scission of the chains. This will in turn make the exposed parts of the polymer more or less prone to dissolve and can thus be used to define patterns in the polymer.

2.5.3 Thin film deposition - Physical Vapor Deposition (PVD)

PVD is a collective term for different techniques that are used to deposit thin films in nanofabrication. In this project, thermal evaporation and sputtering have been used.

In sputtering, noble gas ions are accelerated and collided with a source material. The ion momentum makes the collision so violent that surface atoms or clusters of the source will be ejected from the material. The atoms/clusters will then travel through the sputtering chamber to a target surface where they stick and condense.

Thermal evaporation utilizes heating as means to make surface material leave the source. When enough energy (heat) is provided the surface atoms will be ejected from the source. These atoms will then move from the source to the target where they condense. Important parameters that change the rate of evaporation are temperature of source, and pressure where the source is situated. The thermal energy required to heat the source is usually provided through resistive heating or bombardment of the source with an electron beam.

2.5.4 Hole mask Colloidal lithography (HCL)

A colloid is defined as a substance evenly distributed as microscopic particles in another liquid substance [18], for example the fat particles in milk. Colloidal lithography refers to the use of colloids as a way of doing lithography.

The typical way of doing colloidal lithography is using charged colloidal particles in a solution [19]. The interaction between particles will make them arrange themselves in a way that the total resulting coulomb repulsion is minimized, i.e. the particles will spread out us much as possible. This repulsion will also lead to that the particles will not spontaneously aggregate in the solution. If the particles are made to adhere to a surface the same principle of arrangement does apply due to the interparticle repulsion and thus the particles will form an even distribution of particles on the surface, forming a hexagonal pattern thus maximizing interparticle seperation. Strongly charged particles may arrange themselves in other patterns.

The type of colloidal lithography used in this project is called Hole mask Colloidal Lithography (HCL) [19]. The basic implementation of HCL can be seen in figure 2.9.

Below follows a description how we have implemented the HCL-process. The numbers in the text refer to the different steps in 2.9. Starting off with the substrate. (1). A sacrificial PMMA layer is spun on top of the substrate surface (2). The PMMA is subjected to a short oxygen plasma to increase hydrophilicity and then treated to increase colloidal particle adhesion to the surface. This can be done by using chemical substances that will effectively charge the surface with charge opposite that of the colloidal particles. In this project Poly(diallyl dimethylammonium) chloride (PDDA) was utilized for this purpose. When the colloidal particle solution is applied to the surface (3) the particles will arrange themselves in an even distribution and adhere to the surface, so that when the solution is removed the particles remain on the surface. A thin ($\tilde{2}$0 nm.) layer of Au is deposited on the PMMA and particles (4). When the particles are then removed (5) we will have an etch mask. Removing of the particles can for example be done through tape stripping i.e. using a piece of tape. The sample is then subjected to an O_2-plasma etching process to etch through the exposed PMMA down to the substrate(6). The desired material is then deposited through the mask and the desired structure is obtained on the substrate (7). The last step is the so called lift off (8) where the sample is exposed to acetone which will completely dissolve the PMMA. There are other ways of performing HCL. For example, changing sacrificial layer, mask material, colloidal particles etc.

Undercut is a term that refers to the situation when the diameter of the hole in the PMMA is larger than the hole in the gold mask. It allows for more advanced structures. A couple of examples can be seen in image 2.10. Possibilities include monomers (single particles)(1), cones (2) and dimers (dual particles), where the later utilize the deposition technique called shadow evaporation. A schematic of the shadow evaporation process can be seen in figure 2.11. The cone structure is obtained utilizing a phenomenon that occurs when evaporating thin films. Material will start successively growing on the sides of the mask

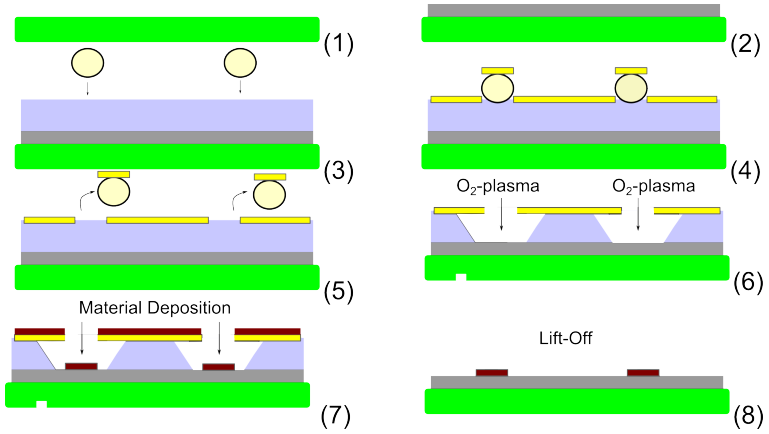

Figure 2.9: Schematic of the different process steps when using Hole mask Colloidal Lithography

edges, for example the holes in the HCL-case. As more and more material is deposited, the diameter of the hole will shrink. Eventually the hole will close as shown in figure 2.10

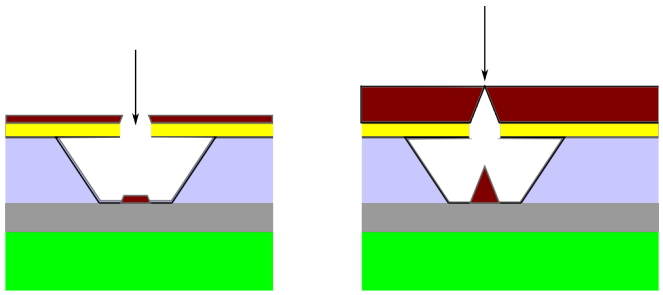

Figure 2.10: Schematic of how cone structures are deposited

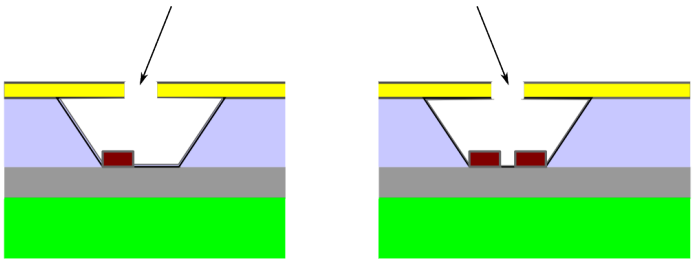

Figure 2.11: Schematic how particle pairs can be fabricated using shadow evaporation

2.6 Characterization Methods

In the following section we will discuss the different characterization-methods used in this project. We will start off by giving a brief introduction to some characterization equipment and explain their working principles. Understanding the working principles is important when it comes to interpreting the resulting data. Readers with previous experience in SEM, SPM, XPS and Mass-spectrometry may skip this section.

2.6.1 Scanning Electron Microscope (SEM)

The SEM is perhaps the most well known of electron microscopes. The working principle is that a high energy electron beam is focused onto the sample surface. Electrons that are ejected from the sample, as a consequence of ionization of surface atoms or scattering events, are detected using different detectors in the chamber. The electron beam moves in a raster scan over the sample surface and an image is generated based on the intensity of electrons ejected from each point.

2.6.2 X-ray Photoelectron spectroscopy (XPS)

XPS utilizes x-ray photons to eject electrons from a sample surface. In short we shoot in a photon with energy high enough to excite and eject core electrons from the target atoms. By detecting the energy of the ejected electrons we obtain the binding energy, which is correlated with the orbital it was excited from. Since orbital energies are material specific we obtain very precise information of surface composition. Photoelectrons are also very quickly absorbed by the material so the electrons ejected and detected are sure to originate from the top few nm of the sample making XPS a very surface sensitive measurement tool.

2.6.3 Mass-spectrometry

The basic working principle of mass spectrometry is ionizing and accelerating sampled gas atoms in an electric field and then let them pass through a magnetic field. Depending on the mass and charge of the ion, it will have different curvature when passing through the magnetic field. By measuring the directions the ions have when they leave the magnetic field, information of the mass/charge ratio can be obtained. Important thing to note; since what we actually detect is the ratio between charge and mass of accelerated ions, a single substance can and will give rise to many mass peaks depending on how it is ionized. For example if the noble gas Ar_{40} is ionized to Ar^+ by ripping away an electron and then accelerated through the electric field it will give a signal on mass 40. However if the Ar atom manages to be ionized to Ar^{2+} it will behave like an ion with mass number 20 and a single positive charge, for example Ne^+_{20} and there will be no way of telling them apart. All substances give rise to a distribution of mass peaks depending on how they are ionized. This is called the cracked mass scheme of the substance. Also worth noting is that this cracking scheme will change with different equipment as well as system parameters such as electric field strength etc. An example of how the cracking schemes can look for CH_4 and CO_2 can be seen in table 2.1

Mass peak/Element	CH_4	CO_2
Main	16 (100%)	44 (100%)
2nd	15 (86%)	28 (11%)
3rd	14 (16%)	16 (9%)
4th	13 (8%)	12 (6%)
5th	12 (2%)	45 (1%)

Table 2.1: Example cracking scheme for methane and CO_2. The percentage values give the expected ratio between signal strength of secondary peaks and the main peak (the mass number of the ions) for a specific mass-spectrometry system.

2.6.4 Optical transmission spectroscopy

Transmission spectroscopy refers to the spectroscopy technique where the light transmitted through a sample is measured and we obtain information as percentage of intensity transmitted as a function of wavelength. When the light interacts with the sample it can either be reflected, absorbed, scattered or transmitted. Absorption events can occur when the wavelength of an incoming photon corresponds to one of the many energy state excitations possible within the sample material. Such events include molecular vibrational- and rotational state excitations, electronic excitations, core electron excitations and so on.

Depending on the sample structure, other more exotic absorption events may occur. For example, localized surface plasmon resonances.

This type of spectroscopy measurement provides information of the optical characteristics of the sample. A specific example would be whether or not we have TiO_2 on the surface. If the sample does indeed have TiO_2 then the sample should absorb light with energy more than $\tilde{3}$ eV very efficiently. It also provides information how the catalyst material interacts with the light.

If the samples show tendencies toward localized surface Plasmon resonances then this will also show up in this type of measurement as a sharp dip in transmission due to absorption and/or scattering of light.

Chapter 3

Experimental approach

3.1 Sample preparation

In this section we will discuss the specifics of how the samples used in this work were fabricated as well as motivate why certain techniques were utilized. The goal of the fabrication is to create samples that exhibit photocatalytic activity. In the background section we discussed that TiO_2 exhibits photocatalytic properties as well as how copper and platinum can serve as catalysts for the desired reactions. The desired structure should thus basically be a flat TiO_2 surface with exposed nanostructured metal catalyst material on top.

3.1.1 Substrate- and TiO_2 preperation

The common denominator of all samples is the way the substrate and the TiO_2 layer were prepared. The substrate is made out of borofloat glass. The reason for this is threefold. Firstly, borofloat is inert, which is critical since we do not want the substrate to participate in, or promote, any chemical reactions of its own. Secondly, glasses are in general good insulators. If the substrate was conducting the excited charge carriers in the photo process could leak into the substrate and escape. Thirdly, borofloat is transparent, opening the opportunity to shine light both from the front and from behind thus opening more possibilities for how and which experiments can be conducted. Of course there are other materials that would serve just as well or better for these purposes. One example would be fused silica which is also a glass but with better light transmission characteristics, especially in the UV-range. However, fused silica is much more expensive and the benefits were determined to not motivate the cost in this work.

The substrate is thoroughly cleaned in a standard degrease process to remove all organic substances from the surface. A five minutes bath in aceton with ultrasonic agitation, then five more minutes in isopropanol (IPA) with ultrasonic agitation and lastly 5 minutes in Milli-q water with ultrasonic agitation. Prior to the deposition of TiO_2 the substrate is also subjected to a strong oxygen plasma strip (500W for 2 minutes in a TePla 300PC microwave plasma system).

A 50 nm thin film of TiO_2 was then sputtered on the substrate. We men-

tioned earlier in the background chapter that sputtered films can be expected to be nanocrystalline or amorphous if untreated. Grain-boundaries introduce trap states in the lattice where photoexcited electrons and holes can become trapped. The smaller the average grain size the more grain-boundaries which in turn leads to more trap states. This can be detrimental to charge transportation properties of the TiO_2 and could lead to less excited charge carriers reaching the surface, thereby decreasing quantum yield of the photocatalyst. The grain size can be increased by thermal annealing which also can be used to change the crystal structure of the TiO_2.

We discussed in 2.3.2 that anatase TiO_2 exhibits better photocatalytic properties for CO_2 reduction and H_2O oxidation. It has been shown that amorphous TiO_2 shows formation of the anatase phase when heated to 400-600°C [20].

The samples with TiO_2 film were therefore thermally treated in 500°C for 5 minutes which would result in an partial anatase film with larger grain size [20].

3.1.2 Catalyst cluster samples

We will now discuss different ways of depositing the catalyst materials Cu and Pt on to the TiO_2. Two different types of structures were used. The first type, which we will call "Catalyst cluster samples", is based on the properties of early growth of material during evaporation. To understand how the result should be we must first discuss film growth. Note that this discussion deals with how material growth occurs under normal conditions during evaporation. Evaporated films do not necessarily grow atom layer by atom layer. In many cases, when depositing metals on insulating supports, it grows atom clusters that eventually form a continuous film [21]. As a conceptual image we allow one atom to reach the surface at a time. When the first atom reaches the surface it will not stick to the position where it landed. The atom will have some time to move around until it finds a trap state or more generally where it is energetically favorably to stick. When the second atom reaches the surface, it too will have time to move around and find a suitable position to stick on the surface. This can either be a different trap state than the first atom or it can be the trap state created by the first atom. As more and more atoms land on the surface the existing clusters of atoms will continue to grow in size or new clusters will be formed. Surface diffusion is dependent on surface material, material being deposited and temperature of substrate, amongst other things. If enough material is deposited on the surface the clusters will grow together, creating a fully covering film of material. But before this happens we will have nanometer sized particles on the surface. This is what we were hoping for and wanted to utilize in these samples.

The samples were fabricated by depositing catalyst material in amounts equivalent to mean thicknesses between 0.5 to 1.5 nm. The aim was to avoid a fully covering film and instead have clusters of catalyst material on the surface. Specifically, the samples were divided into six subgroups:

1. 0.5 nm Cu

2. 0.5 nm Pt

3. 0.5 nm Pt + 0.5 nm Cu
4. 1.5 nm Cu
5. 1.5 nm Pt
6. 1.5 nm Pt + 1.5 nm Cu

It is important to mention that the above mentioned values are only approximate and thicknesses will most likely differ in reality. Possible sources of error include: shutter opening and closing delays in the deposition system, degradation and positioning of thickness monitor and overall precision of the system.

3.1.3 Nanoparticle samples

The second type of sample that was fabricated was the "Catalyst particle sample". The goal was to create well defined particle pair structures schematically shown in figure 3.1.

This was accomplished through HCL processing using the resist A2 PMMA

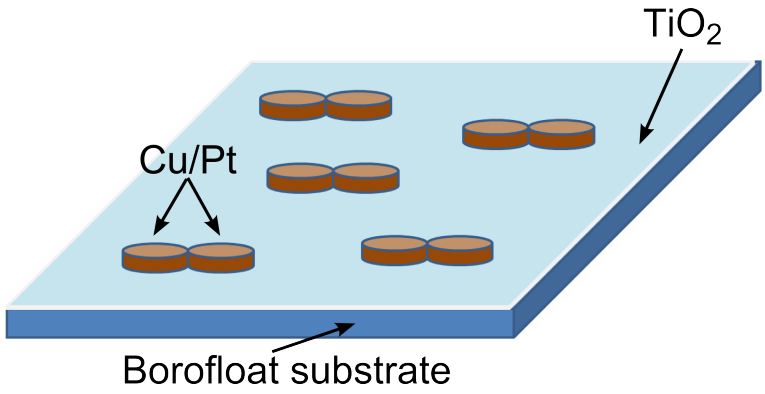

Figure 3.1: Schematic image of the desired structure of catalyst particle samples

950K (Poly(methyl methacrylate) with molecular weight of 950 at 2% concentration in Anisol) as sacrificial layer. The PMMA was spun on the already prepared TiO_2 layer at 1500 rpm, which results in an approximately 100 nm thick layer of PMMA. The samples were then baked on a hot plate at 170°Cfor 10 min. The PMMA was then subjected to a short oxygen plasma to increase hydrophilicity after which the PMMA was treated with PDDA (poly(diallyldimethylammonium chloride)) solution for 45 sec to increase colloidal particle adhesion. The sample was then rinsed with Milli-q water and blow dried with nitrogen to remove leftover PDDA solution. This step was repeated for the colloidal particle solution for 60 seconds after which the sample was rinsed and dried again. Colloidal particles used were charged, spherically shaped polystyrene particles (PS-particles) with a diameter of approximately 110 nm. The PS-solution had a PS-concentration of approximately 0.2% and 0.1mM NaCl. A 20 nm gold film was then deposited on top of the PMMA creating an etch mask. After this the PS-particles were removed through tape-stripping. A somewhat directional oxygen plasma was then used to etch through

the sacrificial layer and create a wide undercut. This corresponds to (6) in figure 2.9

Using thermal evaporation, the twin catalyst particle structure was obtained by depositing materials through shadow evaporation. The samples were divided into three subgroups:

1. 2 x 20 nm Pt at ± 13 degrees
2. 2 x 20 nm Cu at ± 13 degrees
3. 20 nm Pt at +13 degrees, 20 nm Cu at -13 degrees

Approximate evaporation pressures were 4-5·10^{-6} mBar for Pt and 3·10^{-6} mBar for Cu.

3.1.4 Catalytic characterization

The catalytic characterization aims to investigate the actual catalytic properties of the samples. I.e. measuring what possible effect the photocatalyst has on introduced reactants, in this case CO_2 and H_2O. The goal is to obtain information on product formation and if possible, reaction rates. The basic principle of the experiments is fairly straightforward. Let an active photocatalyst sample come in contact with the reactants CO_2 and H_2O while irradiated with light with energy larger than the bandgap energy of TiO_2, as discussed in 2.4.1, and measure the resulting products using massspectrometry.

The light source used in the experiments, seen in figure 3.2, is a 100 W Hg-lamp with intensity peaks in the UV-region making it suitable for our purposes.

As was discussed in 2.3.2, anatase TiO_2 has a band gap energy of 3.2 eV.

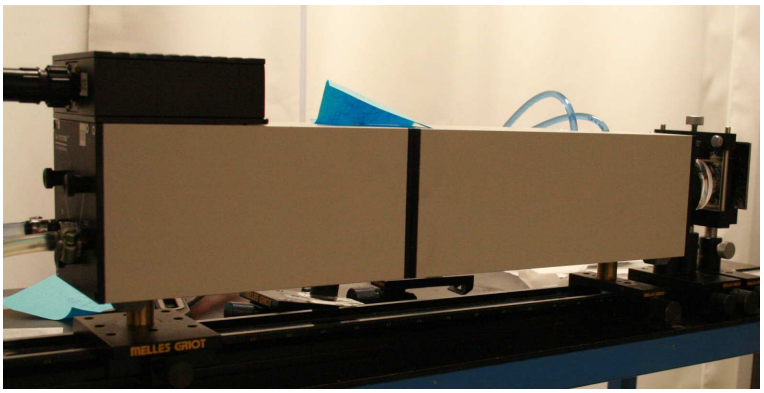

Figure 3.2: UV-Light source used in reactor experiments

Thus light with a wavelength of approximately 380 nm or less is required to create the necessary electron-hole pairs. The intensity spectrum of the Hg-lamp can be seen in figure 3.3

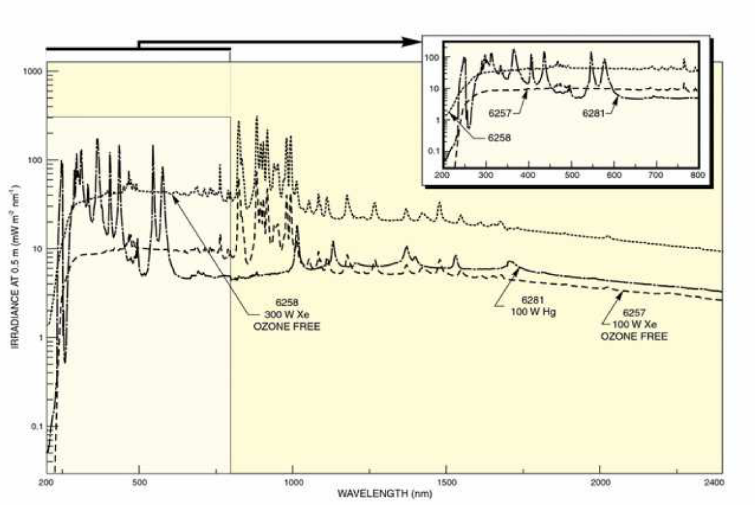

Figure 3.3: Emission spectrum of the 100 W Hg UV-light source used in the reactor experiments

We notice in the figure that a large set of irradiance peaks are in the deep UV-range. The main irradiance peak can be found at approximately 360 nm (figure 3.3 top right).

The reactor experiments can either be performed with reactants in their gas phase or in their liquid phase. We chose to perform the measurements with the reactants in their gas phase due to the production of carbonic acid if CO_2 is dissolved in water. The presence of carbonic acid would lower the pH value and thus shift the redox-potential of the TiO_2 relative to that of the reactants [14].

However carbonic acid does not exist in gas phase under normal conditions which means that we do not have to worry about any of the aforementioned complications. In this project we have used mass spectrometry as detection method in our reactor experiments due to its sensitivity and versatility when doing gas phase measurements.

To control the relative concentrations of gas; two mass flow controllers (MFC) were used. One was used to regulate the flow of Ar-gas and the other was used to regulate the flow of CO_2. The Ar-gas was used as a water carrier as well as a reference signal in the MS. The Ar-gas was led through a water bubbler with Milli-q water. Assuming absolute humidity of the Ar-gas it is possible to calculate the amount of H_2O molecules per unit flow of Ar-gas and thus regulating the H_2O-CO_2 mole-ratio. CO_2-properties were obtained through [22].

Continuous flow reactor measurements

The continuous flow measurement was the first of two methods that were utilized in our attempt to obtain information on the samples photocatalytic properties. A schematic of the measurement setup can be seen in figure 3.4

The basic principle of a continuous flow reactor, as the name implies, is that a

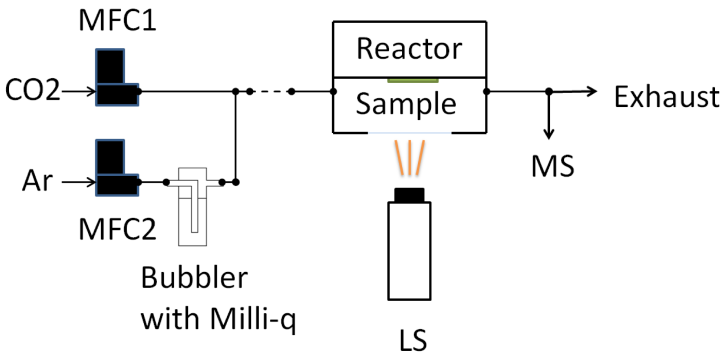

Figure 3.4: Schematic of the continuous flow reactor setup. MS: Mass spectrometer, LS: Lightsource, MFC: Mass flow controller

continuous and constant flow of reactants is streamed through the reactor chamber where the sample is mounted. The sample is then irradiated with UV-light through a window, see figure 3.5. The inflow consists solely of reactants but the outflow will contain some products, too.

Since it is difficult to know how the flow scheme will look inside the reac-

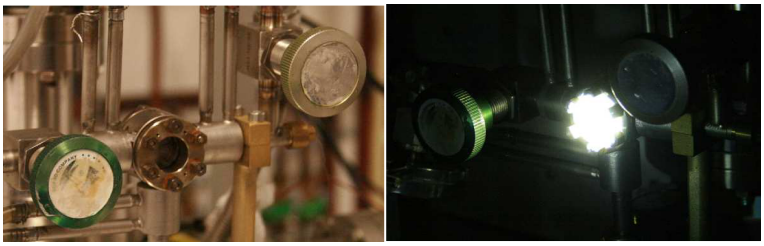

Figure 3.5: Microreactor used for both types of reactor experiments

tor the detection has to take place in the exhaust. The pros of flow mode measurements are that they are very easy to perform and parameters, like reactant concentrations, can be changed during the experiment. The cons are that the reactants will have less time inside the reactor thus having less probability of participating in a redox-reaction. This leads to less products being produced and less signal to detect.

Batch reactor measurements

The second type of measurement performed is the so called Batch reactor measurement. Unlike continuous flow reactor experiments where we send a constant flow of reactants, we now put a fixed amount of reactants inside the reactor with the sample and close it off, sampling from the same "batch" during the whole experiment. The schematic setup can be seen in figure 3.6.

The experiment was performed by streaming a mixture of reactants through

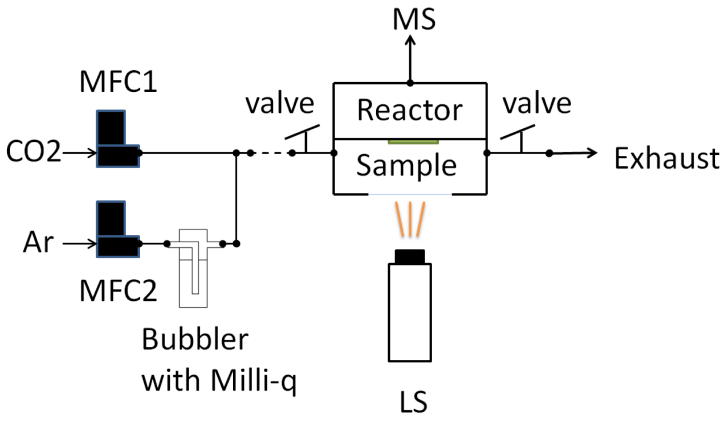

Figure 3.6: Schematic of the batch reactor measurement setup. LS: Light source, MS: Mass spectrometer, MFC: Mass Flow Controller

the reactor until it can be seen as a steady state flow. When a steady state flow can be assumed the valves on both side of the reactor are quickly closed, trapping a "slice" of the gas flow inside the reactor. This slice will have approximately the same pressure and concentration of gases as the original flow. Specifically the flows of CO_2 and Ar were set to 4.804-195.196 ml/min which, according to our calculations result in a molar concentration of approximately 1:1 for CO_2 and H_2O. We then sample from the reactor without light for a couple of minutes, to measure a background signal, after which the UV-source is turned on and the sample irradiated. The pressure inside the reactor was about 600 mBar, at the start of the experiments.

Chapter 4

Results and Discussion

In this chapter the results from the characterization using SEM, XPS, optical characterization and photocatalytical methods will be presented.

4.1 Physical characterization

Images of dual particle samples can be seen in figures 4.1 and 4.2. These samples are dual particles deposited on a Si-substrate to enhance resolution and avoid charging effects that would result from the insulating borofloat substrate. Through inspection of these images the coverage of catalyst material and size of particles was obtained.

The size of the Pt particles was measured to be approximately 105 nm for the first particle and 87 nm for the second particle. The reason why there is a difference in diameter between the particles is that when depositing materials by evaporation, holes, for example, have a tendency to become smaller and smaller. If enough material is deposited the holes will grow shut. This phenomenon is utilized when depositing cone structures by HCL which was described in the background chapter. This also implies that the particles are not cylinder shaped. Instead they are shaped like conical frusta. The total coverage of particles was measured to be approximately 26 %.

The average size of Cu-particles was measured to be approximately 107 nm for the big one and 95 nm for the small one. We notice that the copper particles are a little bit larger than the Pt particles. This can be due to difference in growth properties on the Au mask. In this case it seems like Cu causes the mask to close at a slower rate than Pt. Another possibility is that Cu has greater surface mobility and therefore create larger particles. Therefore the total coverage of copper is somewhat larger than 26%.

We also note that there is a small overlap of about 10 nm of the particles. Overall the particles form a uniform distribution across the samples.

Attempted SEM measurements of particle cluster samples on Si-substrate have not been able to produce any images, due to difficulty in getting enough con-

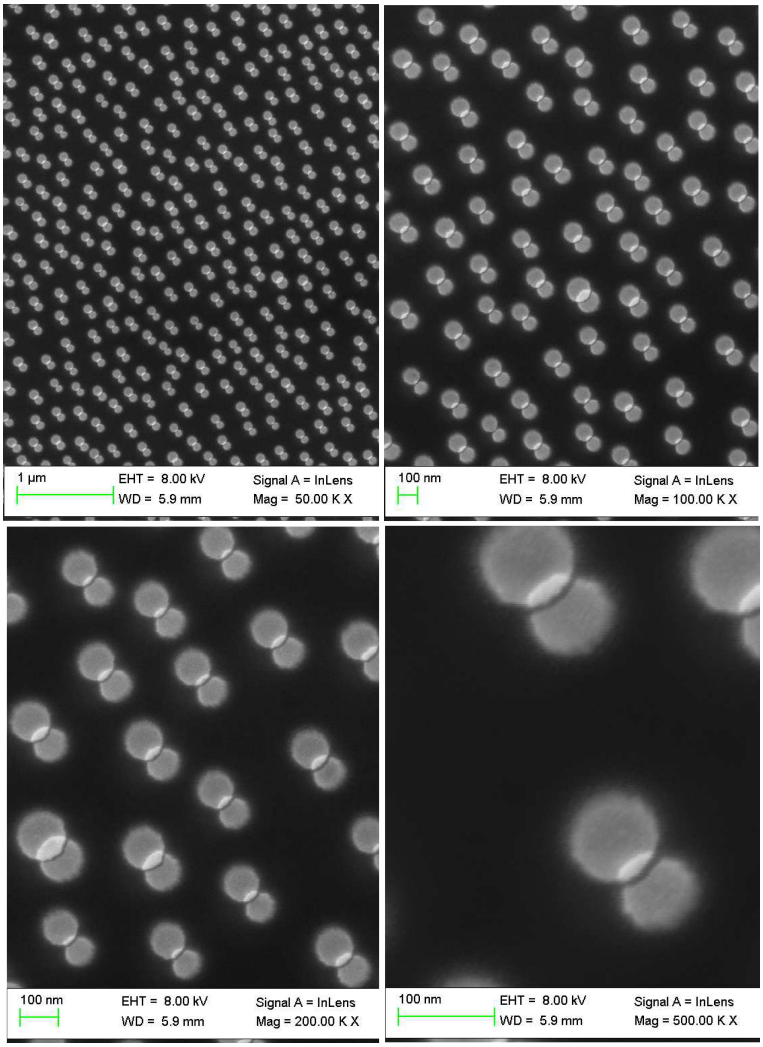

Figure 4.1: SEM-image of a Pt dual-particle sample at different magnifications

trast. This can provide valuable information though since it implies that the surface has very low topography, has a fully covering film of material and/or that the formed particle clusters are too small to be able to provide contrast.

4.2 XPS measurements

There are five elements that can be expected on the sample surfaces. Those elements are Titanium, Oxygen, Copper, Platinum and Carbon. The first four should be there since we put them there in the fabrication process. Carbon is an inevitable contamination that originates from carbon groups present in the atmosphere. Basically anything left in normal atmosphere will end up with a monolayer of carbon contamination on the surface. Such carbon formation is not always undesirable though and it is common practice to account for shifts in

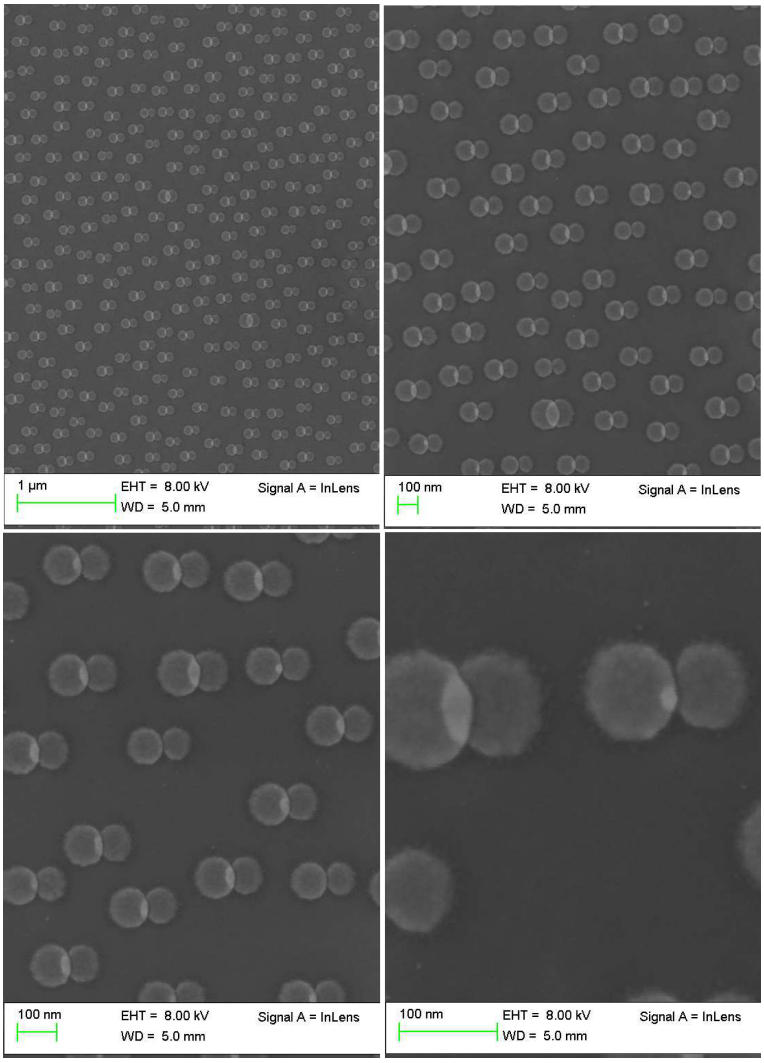

Figure 4.2: SEM-image of a Cu dual-particle sample at different magnifications

the measurements by calibrating using the position of the carbon peak. Carbon binds in different groups on different materials though, so some knowledge is required on the form in which the carbon is bound.

Representative XPS-curves from measurements of the (Ti(2p))-orbital, (Pt(4f))-orbital and (Cu(2p))-orbital can be seen in figures 4.3, 4.4 and 4.5 respectively.

The XPS-curves can provide information on what elements are present on a surface, the atomic concentration of elements on the surface and also which chemical state the element is in. It is possible for example to see if a metal has been oxidized or if it is in metallic phase, by looking at the position of the peak. Depending on which chemical state an element is in the orbital energies can become shifted. Measured curves can also become broader. This is a conse-

quence of more than one chemical state of the same material being present on the surface.

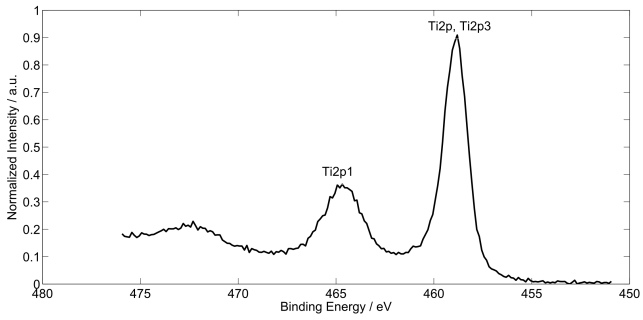

Figure 4.3: Representative graph of the Ti2p orbital region

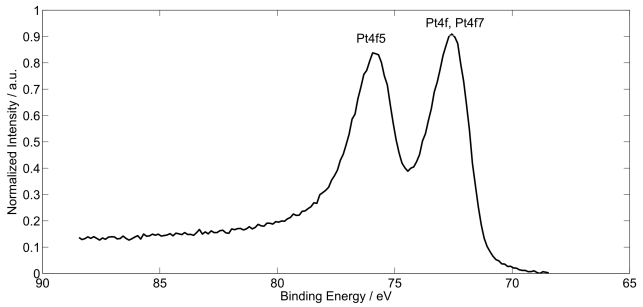

Figure 4.4: Representative graph of the Pt4f orbital region

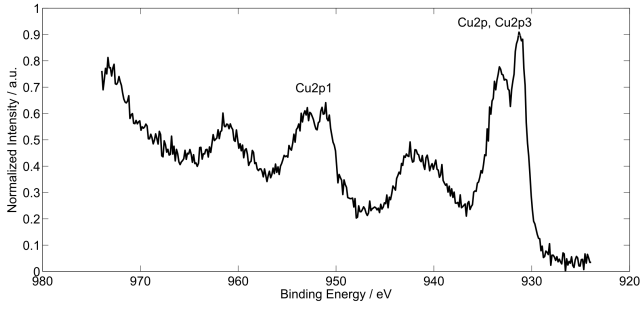

Figure 4.5: Representative graph of the Cu2p orbital region

Both the Ti(2p)-curve and the Cu(2p)-curve are taken from the same sample. Since we did not know which form the carbon was in, we calibrated the measurement by looking at possible chemical states and choosing the one that

describes the result best. We expect the Ti to be bound in the form of TiO_2. When looking in the literature the TiO_2-Ti(2p) peak is found between 458.8-459.2 eV [23]. The Ti(2p) peak was shifted to 459.2 making the Cu(2p)-curve shift accordingly. The Cu(2p)-peak shifted to 933.6 in good agreement where the CuO-peak should be situated [23]. This indicates that we have both TiO_2 on the surface as well as the "native oxide" mentioned in [24]. The native oxide is a mix of different oxide and hydroxide species present on Cu left in normal atmosphere for some time [24]. If using the same interpretation and shifting the Ti(2p) peak to 459.2 eV then the Pt4f curve seen in figure 4.4 is shifted to 72.6 eV whereas the peak for metallic Pt should be found at 71.0-71.2 eV [23]. This suggests that the platinum is in the form of $Pt(OH)_2$ [23]. It is possible that the Pt has bound OH groups to its surface since the samples have been part of photocatalysis experiments. However it is difficult to say whether this is the true origin of the shift.

These curves are pretty much the same for all samples that have the given materials on them. I.e. we expect that the copper on all our samples will form native oxides, given enough time. The Ti2p-peak should be at the same value for all samples since the fabrication process is the same. Since it is in good agreement with the Cu2p peak the results point toward that TiO_2 is present on the surface. Furthermore, the general features in the Cu(2p)-curve is in good agreement with [24], indicating that there is a native oxide on the copper. It is difficult to say whether the interpretation of the Pt(4f)-peak is correct. It is possible that OH-groups could be present on the Pt but the general feature of the curve points toward that the layer is very thick, since the peak is not that broadened and no other peaks can be seen within the given range. I.e. if there was a layer of OH-groups on the surface, as a consequence of photoreactions, then this layer should be very thin. Probably no more than a couple of monolayers thick. The pure Pt underneath would still be visible and give rise to its own set of peaks i.e. we should see traces of multiple chemical states of Pt.

4.2.1 Atomic concentration in particle cluster samples

In this and the next section we will present atomic concentration calculations done on the samples. For the particle cluster samples this characterization is of higher importance since it basically is one of the few techniques available that can be used to characterize the surface since the SEM measurements on the particle cluster samples were not conclusive.

By comparing peak heights and widths and also taking into account sensitivity factors for different elements, it is possible to calculate the relative atomic concentration of elements on a surface. These calculations were handled automatically using MultiPak 6.0A. The calculated atomic concentration for different particle samples can be seen in table 4.1. The first thing to note, if the reader is new to XPS, is the surprising amount of carbon on all the surfaces. This is an unavoidable situation since the samples are stored in normal atmosphere. By looking at the first sample with a only TiO_2. There is about twice the atomic amount of oxygen as there is titanium on the surface. One possible interpreta-

Sample/Element	Ti	Pt	Cu	O	C
1. 50 nm TiO_2	18.9%	—	—	42.6%	38.5%
2. 50 nm TiO_2 + 1.5 nm Pt	4.2%	27.8%	—	23.3%	44.7%
3. 50 nm TiO_2 + 1.5 nm Cu	1.1%	—	12.2%	39.6%	47.1%
4. 50 nm TiO_2 + 1.5 nm Pt + 1.5 nm Cu	0.1%	6.7%	12.5%	46.5%	34.3%
5. 50 nm TiO_2 + 0.5 nm Pt	11.4%	12.0%	—	40.4%	36.2%
6. 50 nm TiO_2 + 0.5 nm Cu	6.6%	—	14.7%	48.6%	30.1%
7. 50 nm TiO_2 + 0.5 nm Pt + 0.5 nm Cu	0.8%	5.8%	24.0%	40.7%	28.7%

Table 4.1: Relative atomic concentration of elements on particle cluster samples. The values are representative.

tion of this result is that the oxygen that gives rise to the signal is bound in the TiO_2 lattice and that there is basically no free oxygen on the surface.

The next thing to note is what we find on line four for the samples with 1.5 nm of both Pt and Cu. There is a vanishingly small signal from Ti. A reasonable explanation is that the deposited metals have created a more or less fully covering film on the surface and there is no exposed TiO_2. It is very likely that there is a similar case with the samples with 1.5 nm Cu or Pt too, i.e. that there is very little or no exposed TiO_2. Also worth noting is that a signal does not mean the same thing as exposed material. Photoelectrons have a short escape depth of about 1-5 nm depending on the surface material. Even if there is a fully covering film, photoelectrons could be registered from 1-5 nm into the surface material. Since the average thickness of catalyst material is only 0.5-3 nm there should still be photoelectrons originating from the TiO_2, ejected from the sample. Therefore it is likely that the small signal that is detected are photoelectrons that managed to penetrate the catalyst layer. The same thing go for all signals, i.e. the 6.7 % of Pt in the Pt/Cu particle cluster sample does not mean 6.7% exposed. The percentages can serve as a hint how the surface looks since it can also point toward crack formation.

We discussed in the background chapter about the growth of films and we mentioned that very thin films tend to be cracked and not fully covering. In that discussion we did not take into account the phenomena of "wetting". Titanium and TiO_2 are very good at wetting metals like Pt and Cu so such films close very rapidly, i.e. even a very thin film can still create a fully covering layer. It is interesting however that even films only 0.5 nm thick can almost completely cover the TiO_2, since it corresponds to only a few monolayers of material.

4.2.2 Atomic concentration in particle samples

In this section we will briefly present the atomic concentration of elements on the particle samples. However we will limit ourselves to only show the relative amount of Ti, Cu and Pt. The values can be seen in table 4.2

Although the results correspond pretty well with the SEM images presented earlier it is important not to mistake the measured values as an area concentration

Sample/Element	Ti	Pt	Cu
50 nm TiO_2 + dual Pt particles	70.55	29.45	—
50 nm TiO_2 + dual Cu particles	63.5	—	36.5

Table 4.2: Relative atomic concentration of elements on dual particle samples. Values are representative

of material like that calculated from the SEM images. I.e. atomic concentration is not the same thing as bulk material concentration. When comparing the coverage calculated from SEM measurement to the ones listed in table 4.2 one sees that the XPS-measurements suggest a slightly higher coverage of catalyst material. The SEM measurements suggested approximately 26% coverage for Pt-particle samples and a little bit more for the Cu-particle samples. When comparing to the values in table 4.2 we see that the difference is approximately 4 percentage points for Pt-samples and in the same order of magnitude for Cu-samples. The difference can be attributed to cluster formation outside the main particles during evaporation.

One thing worth mentioning is that on the dual particle samples, the particles are about 20 nm thick. As was discussed earlier, photoelectrons have an escape depth of 1-5 nm. Photoelectrons originating from the TiO_2 covered by catalyst particles should have no chance penetrating such a thick layer and thus the detected signal should represent pretty well how the surface actually looks.

4.3 Optical properties of particle samples

In this section, the optical properties of the particle samples will be discussed. Points of interest include absorption properties of TiO_2 and position of plasmon resonance peaks if any. The representative transmission spectrums for respective samples can be seen in figure 4.6.

As was discussed in 2.3.2 the band gap energy of TiO_2 is 3-3.2 eV. This corresponds to photons with wavelength less than approximately 380 nm. It becomes clear from figure 4.6 that this indeed is the case for the samples, as a sharp increase in absorption can be seen in that region. This adsorption region seems to be the same for all samples. Thus it is safe to assume that all samples contain TiO_2

The second point of interest mentioned is the presence and position of plasmon resonance peaks if any. The purpose of this project is not to investigate plasmon characteristics of the surfaces but the reason why this is interesting is that current research is ongoing whether plasmon resonances can be used to enhance photocatalytic properties and thus increase quantum yield in semiconductor photocatalysts or to actually drive the photocatalytic process without the normal photo-excitation of the semiconductor. It is desirable to see no plasmon resonances in the vicinity of the emission peaks of the light source. The reason for this is that we want to be sure about the driving mechanisms for the reaction and in this project we are not interested in plasmon induced photocatal-

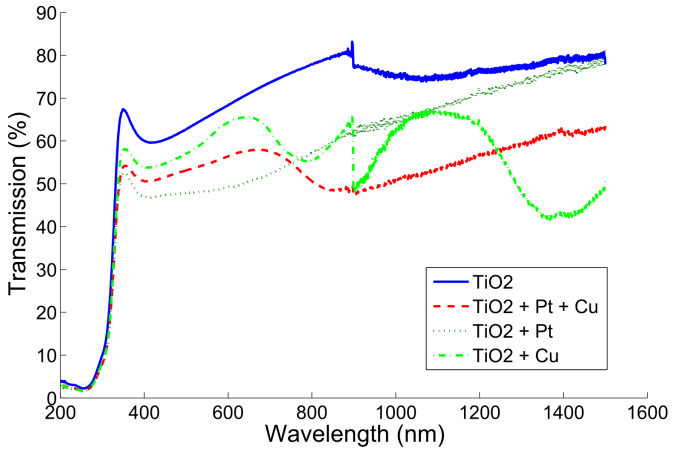

Figure 4.6: Transmission spectrum of catalyst particle samples. Transmission percentage is relative to a reference sample. In this case the reference sample is a clean substrate i.e. borofloat glass, which sets the 100% transmission level.

ysis. If there are any plasmon resonances they would show as a sharp dip in the transmission spectrum. It is not trivial to identify what is a plasmon induced absorption/scattering and what is natural element specific absorption/scattering. In figure 4.7 it is clear that the main Hg emission peaks start in the region just below 600 nm. A reasonable interpretation is that since no sharp transmission dips are present in that region in either of the samples then the above mentioned issue has been avoided. Although plasmon resonances might still be present, the intensity at those wavelengths is sufficiently small so the contribution to total activity is negligible.

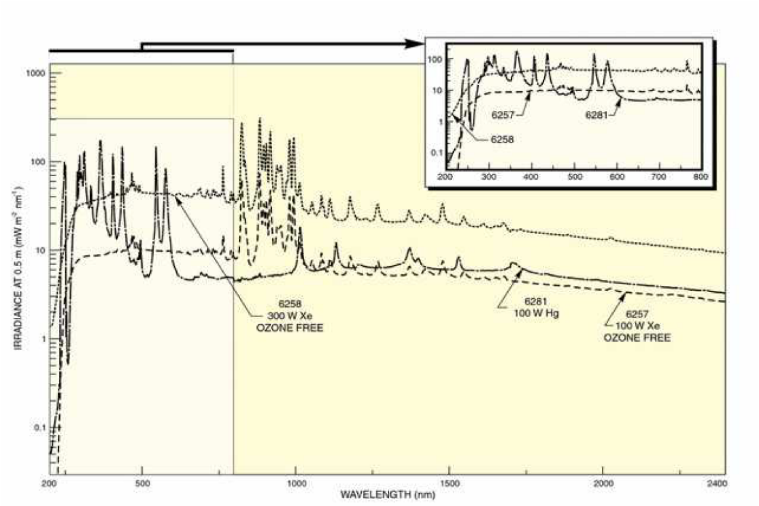

Figure 4.7: Emission spectrum of the 100W Hg-lamp used in reactor experiments

4.4 Reactor experiments

We will now discuss the results from the reactor experiments performed on the samples

4.4.1 Continuous flow reactor experiments

In the continuous flow reactor we realized early on that signals were going to be very weak due to the already known low quantum yield of the photocatalytic reaction but also due to the experimental procedure itself. Since we were not entirely sure of which products we could expect from the reaction it was deemed best to concentrate only on the CO_2-signal to see if it was reduced during the experiment due to photochemical reduction. The samples used in continuous flow reactor measurements were of particle cluster type. A representative figure of all continuous flow reactor experiments can be seen in figure 4.8. The first 10

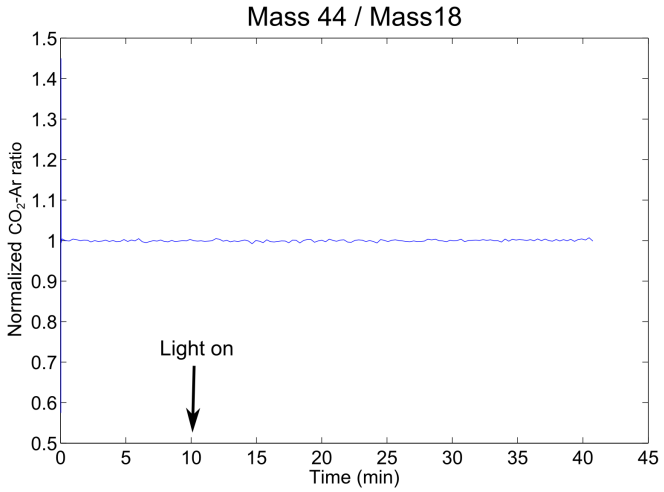

Figure 4.8: Representative measurement curve of the normalized ratio between the CO_2 and Ar-signal. During the first 10 minutes there is no irradiation of the sample. After 10 minutes the UV-source is turned on

minutes of the measurement are without UV-irradiation of the sample. After 10 minutes the UV-source is switched on and the sample is irradiated. The representative curve seen in figure 4.8 does not show any change in signal strength before and after the sample is irradiated. There can be many reasons to why we cannot see any change in signal. The first possible explanation is that the reaction is so slow that we cannot possibly detect such a small change in concentration. Not necessarily only because the MS would have too low precision to detect so small signals but rather that the way data is stored cannot account for such small changes in signal. There is a difference in being able to detect a signal corresponding to a very small concentration C and being able to detect a difference in signals corresponding to the same difference in concentrations. This issue scales with the strength of the original signal. The way the control program of that MS was written may not have allowed for such precision due to lack of significant digits. The data was stored with six significant digits.

This means that the absolute minimum change detectable is of the order of a single ppm, ignoring noise and other limiting factors for the time being. Another possible explanation is that the samples do not show any photocatalytical activity. In the XPS-section we argued that the catalyst material had formed a completely covering film of metal. The interesting question is what implications this has for the photoreaction. The specific question is where the photoreaction takes place. Does it take place on the catalyst material, on the TiO_2 or at the interface between the two? If any part of the reaction can only take place on the TiO_2 or at the interface between TiO_2 and catalyst material, then a fully covering metal film would completely kill the overall reaction. However if the charge carriers can penetrate into the catalyst material and induce a redox-reaction on the metal particles, then a sample with fully covering film will still be able to show photocatalytic activity. Another aspect is that oxidation and reduction may not be able to take place on the same catalyst cluster. I.e. both metals must be in contact with the TiO_2 for a reaction to take place. Unfortunately, the question remains unanswered at this time.

4.4.2 Batch reactor experiments

. In the batch reactor experiments we will concentrate mainly on two signals. The methane signal (mass 15) and the carbon monoxide signal (mass 29). The reason why we only choose those two will be discussed throughout this section. All batch reactor experiments were done on dual particle samples.

Three blank samples were measured during three separate occasions. A blank sample should not have any photocatalytic activity so in order to say that an active sample shows activity it has to produce more signal than the blank samples. Ideally this measurement would not be needed since if samples do not produce a certain substance then the corresponding signal would not change during the experiment. However in reality such a statement is not necessarily true. MS-signals have a tendency to drift sometimes, meaning that signal strengths can increase and decrease over time at a constant sampling concentration. There can be many reasons behind drift. For example, certain substances can stick inside the MS-system making it less sensitive. In order to account for this drift, a blank sample experiment needs to be made.

Figure 4.9 and 4.10 show good reproducibility between measurements meaning that it is safe to assume that these signals can be used to compare with the active samples.

A quick note on data handling and interpretation. The output from the mass-spectrometer is full of noise and very difficult to handle. We assume that the source of noise is mainly of electrical character, for example amplifier noise. Thus the output will be a superposition of the "true" signal and a noise signal. We make the assumption that the noise signal forms a normal distribution. This means that the noise contribution can be eliminated by averaging over enough measurement points. An example of raw output data compared to the averaged signal can be seen in figure 4.11. All post processing of data is then made on the averaged signal. For all calculations and graphs in this project, each point

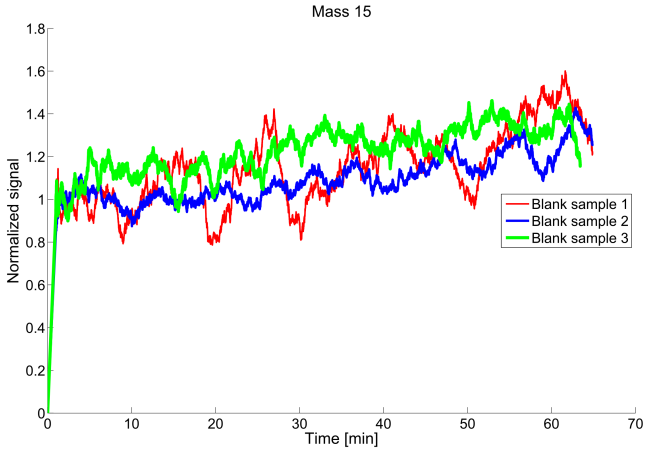

Figure 4.9: Batch reactor measurements on blank samples. The measurements were done a three separate occasions. Mass 15 is a unique cracked mass for methane CH_4. The signal is normalized on the first 1000 cycles of the measurement without irradiation of the sample. Light is turned on at approximately 5 min (1500 cycles).

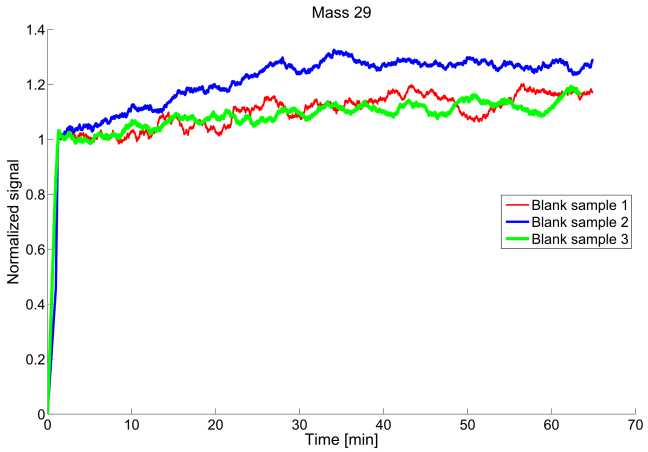

Figure 4.10: Batch reactor measurements on blank samples. The measurements were done a three separate occasions. Mass 29 is a unique cracked mass for CO. The signal is normalized on the first 1000 cycles of the measurement without irradiation of the sample. Light is turned on at approximately 5 min (1500 cycles).

is an average of the 300 nearest points on each side.

CH_4-signal, mass 15

Methane is one of the desired products from photocatalytic CO_2-conversion. It is therefore of interest to see whether our samples have the possibility to produce

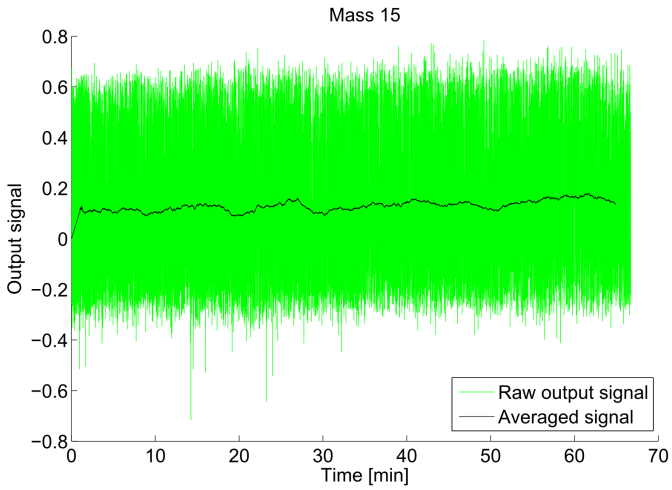

Figure 4.11: The averaged signal in comparison with the same raw output signal of mass 15 of a blank sample.

it. The results can be seen in figures 4.12, 4.13 and 4.14.

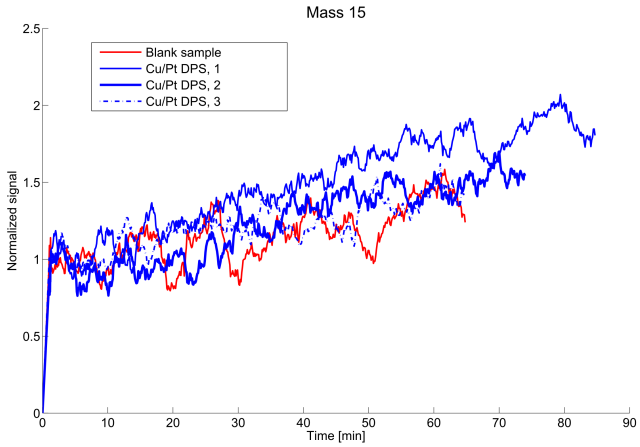

Figure 4.12: Normalized CH_4 signal of Pt/Cu dual particle sample in comparison with blank sample. The signal is normalized on the first 1000 cycles of the measurement without irradiation of the sample. Light is turned on at approximately 5 min (1500 cycles).

It is clear from these measurements that the production of methane is small at best. It is difficult to draw any clear conclusions from these measurements since the signals are so small. This does not necessarily mean that there is no production of methane however, only that the signal is small.

It is noticeable in the figures that the curves of the active samples have a slightly faster average increase in signal strength over time than the blank samples. To

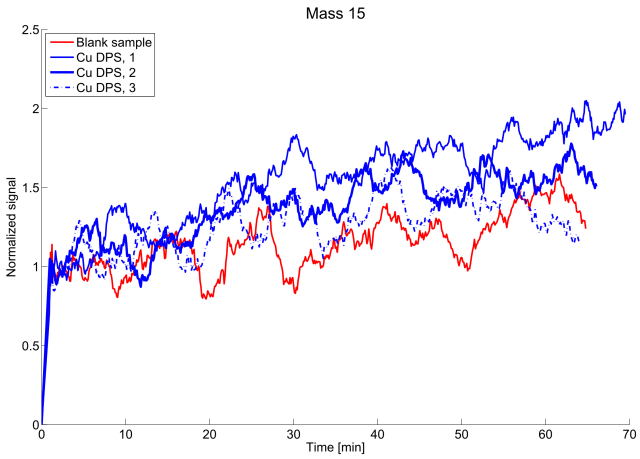

Figure 4.13: Normalized CH_4 signal of Cu dual particle sample (DPS) in comparison with blank sample. The signal is normalized on the first 1000 cycles of the measurement without irradiation of the sample. Light is turned on at approximately 5 min (1500 cycles).

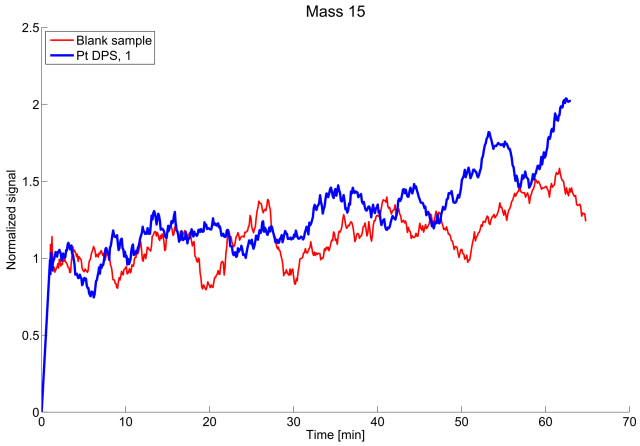

Figure 4.14: Normalized CH_4 signal of Pt dual particle sample (DPS) in comparison with blank sample. The signal is normalized on the first 1000 cycles of the measurement without irradiation of the sample. Light is turned on at approximately 5 min (1500 cycles).

measure the average increase in signal strength over time a linear least square function was fitted to the curves' active regions. The k-value for different samples can be seen in table 4.3 Remarkably, the k-values of the least square fits for active samples are consistently larger than those of the blank samples, by between roughly 50-100%. This tendency can be interpreted as a sign that methane is indeed being produced by the samples. This way of interpreting the data is hardly compelling evidence however and should be considered a possible

Sample	k-value
Blank 1	$1.1827 \cdot 10^{-3}$
Blank 2	$8.814 \cdot 10^{-4}$
Blank 2	$7.674 \cdot 10^{-4}$
Cu/Pt DPS 1	$2.029 \cdot 10^{-3}$
Cu/Pt DPS 2	$1.871 \cdot 10^{-3}$
Cu DPS 1	$2.055 \cdot 10^{-3}$
Cu DPS 2	$1.487 \cdot 10^{-3}$
Pt DPS 1	$2.191 \cdot 10^{-3}$

Table 4.3: Calculated k-values for linear least square fits to measured curves, where k refers to the linear coefficient of the fitted line

tendency rather than irrefutable evidence. For example, we have not taken into account how errors translate through the data processing process.

CO-signal, mass 29

According to the article mentioned in the background chapter [8], the reaction path in electrochemical production of methane and methanol on copper catalysts, involves a CO step where some of the produced CO would be desorbed from the catalyst. Therefore it is of interest to see whether CO is being produced by our samples since this could indicate whether or not the samples show activity and also it would give some small hint whether photocatalysts behave a little bit like electrochemical catalysts.

Representative curves for the mass 29 signal produced by various samples can be seen in figure 4.15. Unfortunately we are not able to detect any CO. There can be numerous explanation to the absence of CO-signal. The first possibility is that no CO is being produced on our samples. This in turn could suggest that the samples does not show any photocatalytic activity.

However TiO_2 based photocatalysts are notorious for having low yield. This is even more of an issue for our samples since our samples' structure has a very small active surface area. The samples may produce CO but the levels are too small to detect or that it reacts further very quickly.

Another plausible explanation to the lack of CO-signal is platinum poisoning. CO binds exceptionally hard to platinum, reducing its catalytical properties and a large amount of energy is needed to remove the CO from the Pt-surface. There could be a small amount of CO being produced by our samples but it never leaves the sample surface due to this reason.

The reason why CO is of interest is because it is assumed that it is a transition state in the electrochemical conversion of CO_2 and water into hydrocarbons. However, the assumption that CO is also a transition state in the photochemical conversion may not necessarily be true.

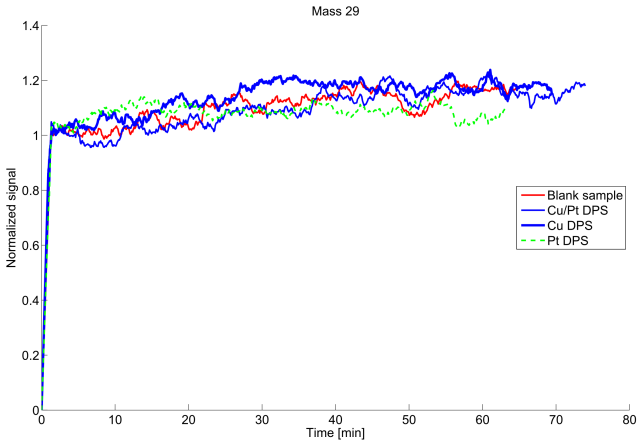

Figure 4.15: Representative curves for mass 29 signal produced by Cu/Pt, Cu and Pt dual particle sample (DPS). The signal is normalized on the first 1000 cycles of the measurement without irradiation of the sample. Light is turned on at approximately 5 min (1500 cycles).

Chapter 5

Summary and Conclusion

This project aimed to investigate whether a well defined sample structure could be used to scrutinize the specifics of light assisted CO_2 conversion into hydrocarbons on TiO_2-based photocatalysts.

In order to achieve this, two types of model catalysts were fabricated. Both of which had ceTiO2 deposited as a flat layer on top of a glass substrate to prevent charge carrier loss through the substrate. The TiO_2 is to act as provider of charge carriers to induce redox-reactions on the surface. The main difference is how added metal catalyst material is added to the system. The first sample type relied on the properties of the growth of evaporated nanometer thick films. Our estimation was that film with thickness of only a few nanometers would not yet have formed a fully covering film and therefore form small material clusters on the surface. The second type was a twin catalyst particle structure fabricated using HCL nanofabrication steps and shadow evaporation techniques. The samples were then characterized and their properties evaluated.

While the first type of sample did not show any visible photocatalytic activity, the other showed very small tendencies toward methane production. However, the levels of produced methane were so small making it difficult to determine the validity of the results. Instead we have provided different ways of interpreting the results.

Even if the results from the reactor experiments performed in this project so far have not been revolutionary for the field it does not mean that the approach to the problem as a whole has been bad. Using well defined sample structures in experiments is always something to strive toward because of the control it offers. With the proposed structures we obtain very well defined structures and good control over the TiO_2 as well as catalyst material. The versatility of the samples open up possibilities to perform a wide spectrum of other experiments that could shed some light on the mechanisms of TiO_2-based photocatalysis.

Chapter 6

Outlooks

Before being able to answer the question of whether these particular sample structures are viable for future research in the field, the questions raised in this project should be addressed. Questions such as interaction between catalyst materials, possible trapping of reactants and their transition states as well as determining the overall degradation of samples over time.

Experiments that could be used to answer some of these questions include reactor experiments with the addition of IR-spectrocopy measurements and FTIR or electrochemistry for the purpose of measuring the presence of bound CO-groups after reactor experiments.

Bibliography

[1] International Energy Agency. Key world energy statistics, 2011.

[2] Solar energy, wikipedia. `http://en.wikipedia.org/wiki/Solar_energy`.

[3] Somnath C. Roy, Oomman K. Varghese, Maggie Paulose, and Craig A. Grimes. Toward solar fuels: Photocatalytic conversion of carbon dioxide to hydrocarbons. *ACS NANO*, 4(3):1259–1278, 2010.

[4] Kamila Kocí, Lucie Obalová, and Zdenek Lacný. Photocatalytic reduction of CO_2 over TiO_2 based catalysts. *Chemical Papers*, 62(1):1–9, 2008.

[5] Dobereiners lamp, wikipedia. `http://en.wikipedia.org/wiki/Dobereiner's_lamp`.

[6] Cassandra G. Freyschlag and Robert J. Madix. Precious metal magic, catalytic wizardry. *Materials today*, 14(4):134–142, 2011.

[7] I. Chorkendorff and J.W. Niemantsverdriet. *Concepts of Modern Catalysis and Kinetics*. Wiley-VCH, 2003.

[8] Andrew A. Peterson, Frank Abild-Pedersen, Felix Studt, Jan Rossmeisl, and Jens K. Nørskov. How copper catalyzes the electroreduction of carbon dioxide into hydrocarbon fuels. *Energy Environ. Sci.*, 3:1311–1315, 2010.

[9] Charles Kittel. *Introduction to Solid State Physics*. John Wiley & Sons Inc., 8 edition, 2005.

[10] Peter Y. Yu. *Fundamentals of semiconductors : physics and materials properties*. Springer, 3 edition, 2010.

[11] Akira Fujishima and Kenichi Honda. Electrochemical photolysis of water at a semiconductor electrode. *Nature*, 238:37–38, 1972.

[12] M. R. Ranade, A. Navrotsky, H. Z. Zhang, J. F. Banfield, S. H. Elder, A. Zaban, P. H. Borse, S. K. Kulkarni, G. S. Doran, and H. J. Whitfield. Energetics of nanocrystalline TiO_2. *Proceedings of the National Academy of Sciences of the United States of America*, 99(Suppl 2):6476–6481, 2002.

[13] Rutile, wikipedia. `http://en.wikipedia.org/wiki/Rutile`.

[14] A. L. Linsebigler, G. Q. Lu, and J. T. Yates. Photocatalysis on TiO_2 surfaces - principles, mechanisms, and selected results. *Chemical Reviews*, 95(3):735–758, 1995.

[15] Anatase, wikipedia. `http://en.wikipedia.org/wiki/Anatase`.

[16] Andrew Mills and Stephen le Hunte. An overview of semiconductor photocatalysis. *Journal of Photochemistry and Photobiology A: Chemistry*, 108:1–35, 1997.

[17] Henderson Michael A. A surface science perspective on photocatalysis. *Surface Science Reports*, 66(6-7):185–297, 2011.

[18] Richard A.L. Jones. *Soft Condensed Matter*. Oxford university press, 2010.

[19] Hans Fredriksson, Yury Alaverdyan, Alexandre Dmitriev, Christoph Langhammer, Duncan S. Sutherland, Michael Zäch, and Bengt Kasemo. Hole-mask colloidal lithography. *Advanced Materials*, 19:4297–4302, 2007. Explains the colloidal lithography method.

[20] Raja Sellappan, Jiefang Zhu, Hans Fredriksson, Rafael S. Martins, Michael Zäch, and Dinko Chakarov. Preparation and characterization of TiO_2/carbon composite thin films with enhanced photocatalytic activity. *Journal of Molecular Catalysis A: Chemical*, 335(1-2):136–144, 2011.

[21] John A. Venables. *Introduction to Surface and Thin Film Processes*. Cambridge university press, 2000.

[22] CO_2 properties online. `http://www.carbon-dioxide-properties.com`.

[23] John F. Moulder, William F. Stickle, Peter E. Sobol, and Kenneth D. Bomben. *Handbook of X-ray Photoelectron Spectroscopy*. Physical Electronics, 1992.

[24] Mark C. Biesinger, Leo W. M. Lau, Andrea R. Gerson, and Roger St C. Smart. Resolving surface chemical states in xps analysis of first row transition metals, oxides and hydroxides: Sc, ti, v, cu and zn. *Applied Surface Science*, 257(3):887–898, 2010.